

Supplementary Information

Electron correlation effects on uranium isotope fractionation in U(VI)-U(VI) and U(IV)-U(VI) equilibrium isotopic exchange systems

Ataru Sato,^{ab} Masahiko Hada^a and Minori Abe^{*ab}

^a Department of Chemistry, Graduate School of Science, Tokyo Metropolitan University, 1-1

Minami-Osawa, Hachiojii-shi, Tokyo 192-0397, Japan

^b Department of Chemistry, Graduate School of Advanced Science and Engineering, Hiroshima

University, 1-3-1 Kagamiyama, Higashi-Hiroshima City Hiroshima, 739-8526, Japan

*Email: minoria@hiroshima-u.ac.jp

Contents

- S1.** Dependence of $\ln K_{\text{IV}}$ on solvation effects during geometry optimization
- S2.** Dependence of electron correlation calculations on the number of virtual MOs
- S3.** Basis set dependence of $\ln K_{\text{IV}}$
- S4.** Results of Mulliken population analysis to confirm the oxidation states
- S5.** Comprehensive analyses of CASPT2 and RASPT2 results
- S6.** Electronic energies of the ground and low-lying states
- S7.** Configuration analysis of FSCCSD results
- S8.** T_1 , T_2 amplitudes obtained from CCSD calculations for UCl_4

S1. Dependence of $\ln K_{\text{nv}}$ on solvation effects during geometry optimization

Because the DIRAC software does not incorporate solvation effects within a two-component relativistic Hamiltonian, such effects were explored only during geometry optimizations. These optimizations were carried out in either the gas phase or in water as a solvent, employing the polarizable continuum model (PCM)¹ within the Gaussian09 software package.² The molecular systems used in this analysis included di-nuclear complexes and the $\text{H}_{26}\text{CaU}(\text{PO}_4)_{10}^{2+}$ cluster model, both derived from our previous study.³ The differences in the $\ln K_{\text{nv}}$ values for molecules optimized in the gas phase and in water were relatively small, ranging from 0.02 to 0.39 ‰ (Fig. S1). Hence, the solvation effect on geometry is thought to have had only a minor impact on $\ln K_{\text{nv}}$.

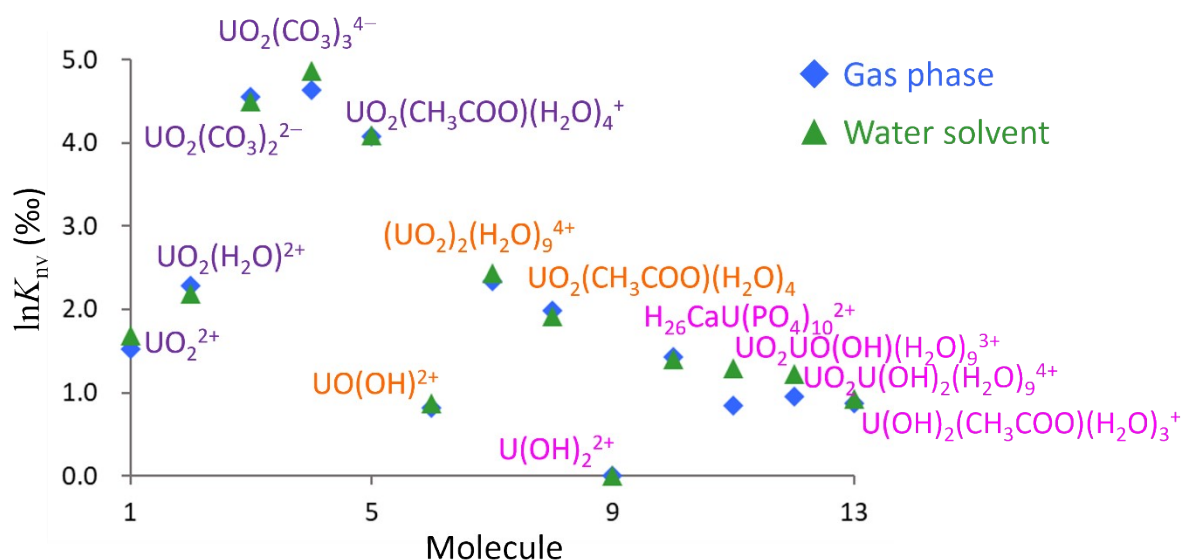


Figure S1. Variations in $\ln K_{\text{nv}}$ as a consequence of applying the solvation effect during geometry optimization. The blue diamonds and green triangles depict $\ln K_{\text{nv}}$ values for molecules optimized in the gas phase and in water as a solvent, respectively. The chemical formulae of the U(VI), U(V) and U(IV) species are provided in purple, orange and pink font, respectively. $\text{U}(\text{OH})_2^{2+}$ was used as a reference when estimating $\ln K_{\text{nv}}$.

S2. Dependence of electron correlation calculation on the number of virtual MOs

The effects of selected molecular orbitals (MOs) on $\ln K_{\text{nv}}$ values were assessed by performing a series of $\ln K_{\text{nv}}$ calculations while varying the range of orbital energies for the virtual MOs included in the correlation calculations. In these trials, $\text{UO}_2\text{F}_4^{2-}$ and $\text{UO}_2(\text{H}_2\text{O})_4^{2+}$ were modeled within the U(VI) systems while UF_4 was modeled in the U(IV) system. Specifically, we computed $\ln K_{\text{nv}}$ values for the $\text{UO}_2\text{F}_4^{2-}/\text{UF}_4$ and $\text{UO}_2\text{F}_4^{2-}/\text{UO}_2(\text{H}_2\text{O})_4^{2+}$ combinations as hypothetical systems. Because of the minor dependence of the results on the basis sets that were used, the combination of basis sets labeled as **(A)** as described in Section S3 was used.

The corresponding results are presented in Table S1. It is noteworthy that including virtual MOs with orbital energies of up to $20.0 E_{\text{h}}$ yielded indistinguishable results from those obtained with MOs having an orbital energy of $100.0 E_{\text{h}}$. On this basis, virtual MOs with orbital energies of up to $20.0 E_{\text{h}}$ were employed in the correlation calculations presented in the main text of the present study.

Table S1 The effect of the selection of virtual MOs included in the correlation calculations on $\ln K_{\text{nv}}$. All the values are shown in units of ‰. The first column in the table indicates the maximum threshold of the orbital energies, in units of E_{h} .

$\text{UO}_2\text{F}_4^{2-}/\text{UF}_4$					
Threshold of orbital energy (E_{h})	$\ln K_{\text{nv}}$ (‰)				
	CCSD	CCSD(T)	FSCCD	CASPT2	RASPT2
1.0	2.88	2.75	1.70	2.71	2.71
2.0	3.08	2.97	1.98	2.79	2.78
3.0	3.13	3.01	2.15	2.84	2.82
4.0	3.16	3.03	2.15	2.83	2.81
5.0	3.07	2.94	2.02	2.72	2.69
6.0	3.07	2.94	1.89	2.72	2.70
7.0	3.09	2.95	1.92	2.73	2.70
8.0	2.95	2.79	1.84	2.57	2.54
9.0	3.00	2.85	1.84	2.62	2.59
10.0	3.00	2.85	1.84	2.62	2.59
20.0	3.08	2.94	1.93	2.71	2.68
50.0	3.08	2.94	1.93	2.71	2.68
100.0	3.08	2.94	1.93	2.70	2.68

$\text{UO}_2\text{F}_4^{2-}/\text{UO}_2(\text{H}_2\text{O})_4^{2+}$				
Threshold of orbital energy (E_{h})	$\ln K_{\text{nv}}$ (‰)			
	MP2	CCSD	CCSD(T)	
1.0	0.95	1.03	0.94	
2.0	1.10	1.15	1.09	
3.0	1.15	1.20	1.14	
4.0	1.28	1.33	1.28	
5.0	1.14	1.19	1.13	
6.0	1.15	1.19	1.13	
7.0	1.14	1.20	1.14	
8.0	1.10	1.16	1.10	
9.0	1.04	1.11	1.03	
10.0	1.04	1.11	1.03	
20.0	1.14	1.20	1.14	
50.0	1.14	1.20	1.14	
100.0	1.14	1.20	1.14	

S3. Basis set dependence of $\ln K_{\text{nv}}$

To examine the correlation between $\ln K_{\text{nv}}$ and the choice of basis sets, $\ln K_{\text{nv}}$ calculations were conducted using various theoretical frameworks. The Hartree-Fock (HF), density functional theory (DFT), second-order Møller-Plesset perturbation (MP2) theory,^{4,5} coupled-cluster theory (CCSD, CCSD(T))^{6,7} and Fock-space CCSD (FSCCSD)⁸ methods were employed, using the exact two-component (X2C) relativistic Hamiltonian⁹⁻¹² for all methods. These calculations were performed using different combinations of basis sets as follows.

(A) Dyall.cv2z¹³ for U and 6-31+G(d)¹⁴⁻¹⁷ for the remaining atoms

(B) Dyall.cv2z for U and Dyall.acv2z¹⁸ for the remaining atoms

(C) Dyall.cv3z¹³ for U and Dyall.acv2z for the remaining atoms

(D) Dyall.cv3z for U and Dyall.acv3z¹⁸ for the remaining atoms

The quadruple zeta basis set was not examined because it is computationally demanding and impractical for the larger real systems. The present DFT calculations utilized the B3LYP hybrid exchange-correlation functional.¹⁹⁻²¹ Because both the complete active-space second-order perturbation (CASPT2)²²⁻²⁴ and restricted active-space second-order perturbation (RASPT2)²⁵ theories have substantial computational demands and are impractical with large basis sets for moderately sized molecules, we refrained from conducting the analysis using these methods. This work modeled UO_2F_2 and UO_2^{2+} as the U(VI) compounds and UF_2^{2+} as the U(IV) compound and calculated $\ln K_{\text{nv}}$ values for the $\text{UO}_2^{2+}/\text{UF}_2^{2+}$, $\text{UO}_2\text{F}_2/\text{UF}_2^{2+}$ and $\text{UO}_2\text{F}_2/\text{UO}_2^{2+}$ systems. During the HF calculations for UF_2^{2+} , the open-shell MOs were treated using an average-of-configuration (AOC) procedure. MP2 calculations were not carried out for UF_2^{2+} because the associated MOs may not always be semi-canonical as assumed in the MP2 method when implemented in DIRAC in open-shell systems. Because of the computational demands associated with employing triple-zeta basis sets for all atoms, calculations using the **(D)** combination were feasible only for UO_2^{2+} and UF_2^{2+} . All $\ln K_{\text{nv}}$ calculations were performed using the DIRAC21 software package^{26, 27} and the geometry

optimization of the molecular models followed the methodologies outlined in the computational details section of the main text.

During the electron correlation calculations, the correlating electrons were considered to be those in occupied MOs ranging from the predominant U 6s orbital to the highest occupied MO. Because there is an energy gap between the virtual MO with an orbital energy of approximately $50 E_h$ and the subsequent MO, virtual MOs having orbital energies lower than $55.0 E_h$ were included in the correlation calculations.

The resulting $\ln K_{nv}$ values are presented in Table S2. The nearly identical results obtained across all the basis sets that were employed suggest that the $\ln K_{nv}$ value is only minimally affected by the selection of basis sets. Based on this survey, basis set (A) was utilized throughout this work; however, exceptionally for hydrogen, the 6-31++G(d,p) was used instead of the 6-31+G(d) to include additional polarization functions.

Table S2 The effect of basis sets on $\ln K_{nv}$. All values shown are in units of permil (‰).

$\text{UO}_2^{2+}/\text{UF}_2^{2+}$	HF(AOC)	B3LYP	CCSD	CCSD(T)	FSCCSD
(A)	1.51	1.19	1.00	1.07	0.81
(B)	1.51	1.19	0.98	1.07	1.00
(C)	1.50	1.18	1.07	0.98	0.79
(D)	1.49	1.18	1.02	1.02	0.77

$\text{UO}_2\text{F}_2/\text{UF}_2^{2+}$	HF(AOC)	B3LYP	CCSD	CCSD(T)	FSCCSD
(A)	3.49	2.68	2.90	2.87	2.71
(B)	3.50	2.69	2.87	2.88	2.88
(C)	3.50	2.68	2.96	2.78	2.68

$\text{UO}_2\text{F}_2/\text{UO}_2^{2+}$	HF	B3LYP	MP2	CCSD	CCSD(T)
(A)	1.98	1.49	1.75	1.90	1.80
(B)	1.99	1.49	1.82	1.89	1.81
(C)	2.00	1.50	1.82	1.89	1.81

S4. Results of Mulliken population analysis to confirm the oxidation states

Table S3 Results of Mulliken population analysis using RECP-B3LYP, X2C-HF and X2C-B3LYP calculations for all U(IV) species considered in the present study. The oxidation states (OSs) of each U are shown in parentheses. Note that the values obtained from RECP calculations are the total spin densities of U whereas the X2C values are the sum of the Mulliken populations of U *5f* orbitals in the open-shell orbitals. The results for U(VI) species are not shown because the calculations for these species were conducted assuming closed shells and the OSs were inevitably +VI.

Molecule	RECP-B3LYP	X2C-HF	X2C-B3LYP
UF ₄	1.97 (IV)	1.93 (IV)	1.79 (IV)
UCl ₄	2.11 (IV)	1.95 (IV)	1.83 (IV)
UBr ₄	2.14 (IV)	1.95 (IV)	1.81 (IV)
U(H ₂ O) ₉ ⁴⁺	2.05 (IV)	1.98 (IV)	1.91 (IV)
U(OH)(H ₂ O) ₈ ³⁺	2.06 (IV)	1.96 (IV)	1.89 (IV)
UCl(H ₂ O) ₈ ³⁺	2.04 (IV)	1.97 (IV)	1.88 (IV)
U(SO ₄)(H ₂ O) ₇ ²⁺	2.08 (IV)	1.96 (IV)	1.87 (IV)
U(SO ₄) ₂ (H ₂ O) ₆	2.08 (IV)	1.97 (IV)	1.89 (IV)

S5. Comprehensive analyses of CASPT2 and RASPT2 results

The $\text{UO}_2\text{Cl}_4^{2-}/\text{UCl}_4$ system, which is the primary focus of the U(IV)-U(VI) system in the main text, was analyzed. Initially, the effect of the improved virtual orbital (IVO) technique on the CASPT2 and RASPT2 calculations was examined. In the case of the CASPT2 process, the inclusion of the IVO method did not alter the total energy when specifying the six $5f_{5/2}$ spinors (i.e., the open-shell spinors in the AOC) in the complete active space (CAS) (Table S4). This lack of an effect is ascribed to the fact that the secondary orbitals are unitarily transformed during the block diagonalization of the Fock matrix for the CAS configuration interaction (CASCI) in the CASPT2 algorithm, which cancels the effect of the IVO approach when the secondary space and the virtual space are identical. When extending the CAS to encompass virtual MOs, the IVO approach affected the total energy and $\ln K_{\text{nv}}$. However, during the CAS (2e, 18s) calculations, intruder state problems seemed to occur, as indicated by the low weight of the 0th-order function, despite using the IVO technique.

Table S4 The effect of incorporating the IVO method and virtual spinors into the CAS during CASPT2 calculations. Here, total energy values and $\ln K_{\text{nv}}$ are given in units of E_{h} and %, respectively. The total energy values for UCl_4 and $\ln K_{\text{nv}}$ values for the $\text{UO}_2\text{Cl}_4^{2-}/\text{UCl}_4$ system are provided. The CAS calculations involving two electrons in six spinors are denoted here as “CAS (2e, 6s).”

CAS configuration (# of virtual spinors in CAS)	Without IVO		With IVO	
	CAS (2e,6s) (0 virtual spinors)	CAS (2e,6s) (0 virtual spinors)	CAS (2e,14s) (+8 virtual spinors)	CAS (2e,18s) (+12 virtual spinors)
Total Energy ²³⁵ U	-29883.5334420700	-29883.5334420700	-29883.531882303	-29883.5328617215
Total Energy ²³⁸ U	-29883.4298385574	-29883.4298385574	-29883.428278785	-29883.4289116926
Weight of 0 th function ²³⁵ U	0.740	0.740	0.742	0.105
Weight of 0 th function ²³⁸ U	0.740	0.740	0.742	0.208
$\ln K_{\text{nv}}$	1.76	1.76	1.66	-365.52

In the case of the RASPT2 method, a calculation without the IVO technique resulted in an exceptionally low weight for the 0th function, indicating a breakdown in the calculation process. Consequently, an anomalous value for $\ln K_{\text{nv}}$ was generated (Table S5). For this reason, it appears

that the IVO method is required to ensure the stability and accuracy of calculations when using the RASPT2 approach.

Table S5 The effect of the IVO technique on RASPT2 calculations. Here total energy and $\ln K_{\text{nv}}$ are given in units of E_h and %, respectively. The total energy values for UCl_4 and $\ln K_{\text{nv}}$ values for the $\text{UO}_2\text{Cl}_4^{2-}/\text{UCl}_4$ system are provided.

		Without IVO	With IVO
Total energy	^{235}U	-29883.5309668732	-29883.5322921448
	^{238}U	-29883.4132473257	-29883.4286886233
Weight of 0 th function	^{235}U	0.00190	0.743
	^{238}U	0.00723	0.743
$\ln K_{\text{nv}}$		-14956.18	1.66

Subsequent work explored the effect of RAS variations on $\ln K_{\text{nv}}$ by altering the RAS configuration for UCl_4 (Table S6). Although the ground state of UCl_4 had three degenerate states associated with A and B irreducible representations (irreps) at the CASCI level, we selected irrep A for the RASCI and RASPT2 calculations because this provided lower energy values compared with irrep B for the RASCI method. The specification of twelve spinors as the RAS3 provided an anomalous value for $\ln K_{\text{nv}}$ despite the moderate weight of the 0th function. Conversely, assigning four and eight spinors as the RAS3 yielded a moderate $\ln K_{\text{nv}}$ value. To assess the potential numerical errors in cases in which four or eight spinors were designated as the RAS3, the relationship between the variations in the mean-square charge radius ($\langle r^2 \rangle$) and $\ln K_{\text{nv}}$ for the isotopes ^{233}U , ^{235}U , ^{236}U and ^{238}U was examined (Fig. S2). In the absence of numerical errors, $\ln K_{\text{nv}}$ should be proportional to $\langle r^2 \rangle$. This proportional relationship was observed when eight spinors were specified as the RAS3 but not in any other case, confirming the absence of numerical errors in the case that eight spinors were specified as the RAS3. Consequently, eight spinors were employed as the RAS3 in the RASPT2 calculations for U(IV) molecules, as detailed in the main text.

Table S6 The effects of RAS3 variations on $\ln K_{\text{nv}}$ for UCl_4 . Total energy is in units of E_h while $\ln K_{\text{nv}}$ is in units of ‰.

# of RAS3 spinors		4	8	12
Total energy	^{235}U	-29883.5330944118	-29883.5322921448	-29884.2614738450
	^{238}U	-29883.4294915040	-29883.4286886233	-29884.1578522807
Weight of 0 th function	^{235}U	0.741	0.743	0.847
	^{238}U	0.741	0.743	0.847
$\ln K_{\text{nv}}$		2.31	1.66	-17.46

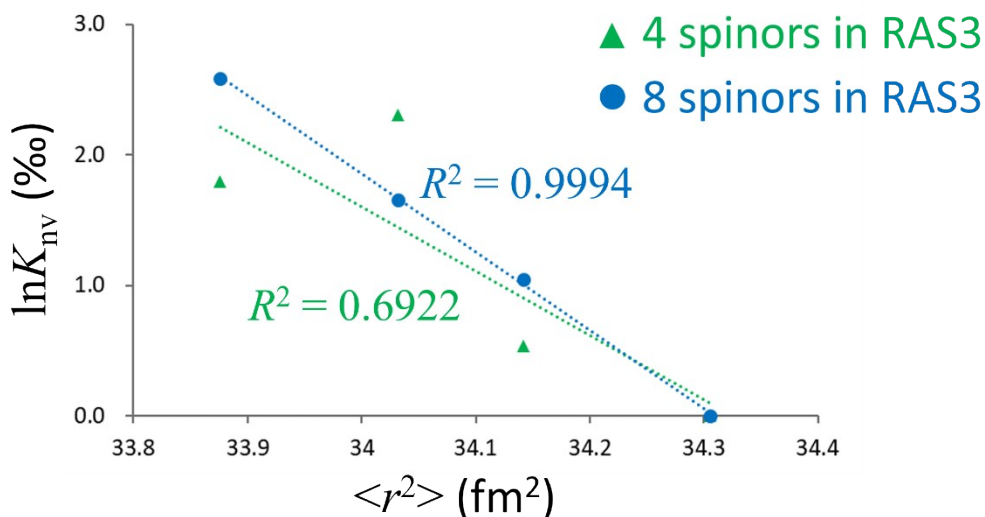


Figure S2. Relationship between $\langle r^2 \rangle$ and $\ln K_{\text{nv}}$ for the isotopes ^{233}U , ^{235}U , ^{236}U and ^{238}U . The horizontal axis shows $\langle r^2 \rangle$ in units of fm^2 whereas the vertical axis shows $\ln K_{\text{nv}}$ in units of ‰. The green triangles and blue circles correspond to data obtained using four and eight spinors as the RAS3, respectively. The dotted lines indicate linear regressions for each set of data, with the coefficient of determination (R^2) displayed alongside each regression line.

Finally, we verified the numerical errors in CASPT2 by varying the irrep and the CI state. To validate the choice of irrep, the relationship between $\langle r^2 \rangle$ and $\ln K_{\text{nv}}$ for various isotopes was examined in conjunction with two irreps. To ensure a comprehensive comparison, calculations were conducted using the HF, B3LYP, CCSD, CCSD(T), CASCI and FSCCD methods in addition to the CASPT2 approach (Fig. S3). The results confirmed that numerical errors were exclusive to the CASPT2 calculations with irrep B. Consequently, irrep A was adopted for all subsequent CASPT2 calculations as described in the main text. Following this, $\ln K_{\text{nv}}$ calculations at the CASPT2 level were performed for three states with the CASCI process and each irrep to assess the correlation

between $\ln K_{\text{nv}}$ and $\langle r^2 \rangle$ (Fig. S4). In the case of irrep A, CASCI states 2 and 3 were found to be degenerate while calculations involving irrep B indicated that states 1 and 2 exhibited degeneracy. The numerical errors observed in these degenerate states confirmed that the degeneracy associated with the CASCI procedure contributed to numerical errors. Therefore, it appears that the numerical errors in CASPT2 calculations with irrep B may be attributed to the degeneracy in the CASCI results.

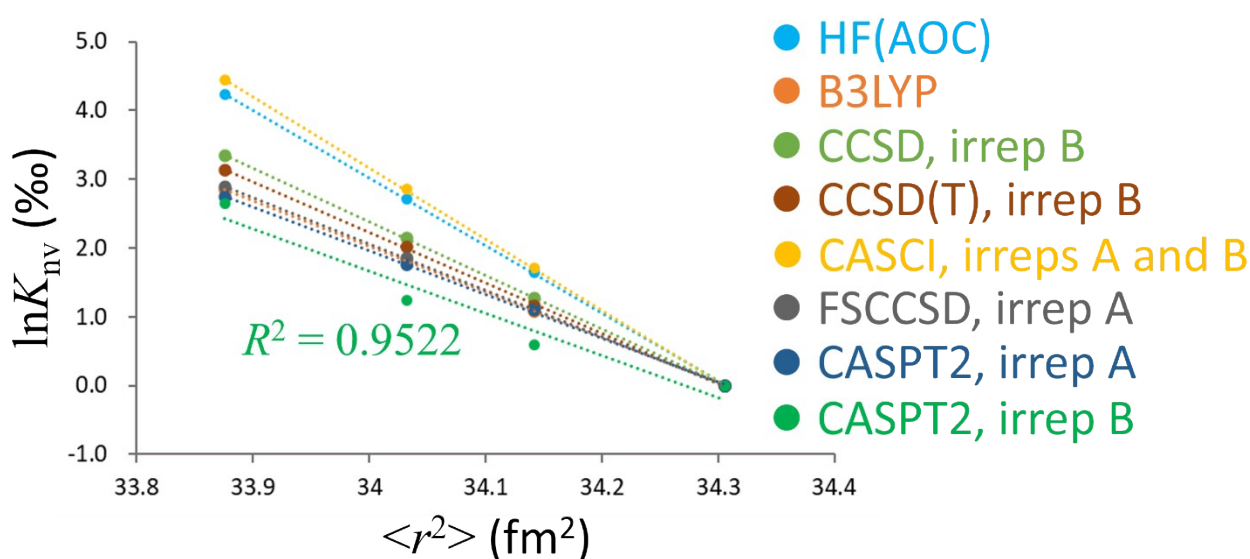


Figure S3. Relationships between $\langle r^2 \rangle$ and $\ln K_{\text{nv}}$ for the isotopes ^{233}U , ^{235}U , ^{236}U and ^{238}U as calculated using the HF, B3LYP, CCSD, CCSD(T), CASCI, FSCCD and CASPT2 methods. The horizontal axis shows $\langle r^2 \rangle$ in units of fm^2 and the vertical axis shows $\ln K_{\text{nv}}$ in units of %. The light blue, orange, yellowish green, brown, yellow, gray, blue and green plots depict data for the HF, B3LYP, CCSD, CCSD(T), CASCI, FSCCD and CASPT2 methods, respectively. The dotted lines indicate linear regressions for each set of data. Only the R^2 value for the CASPT2 results obtained with irrep B is displayed alongside the regression line, as R^2 values for all other methods exceeded 0.999.

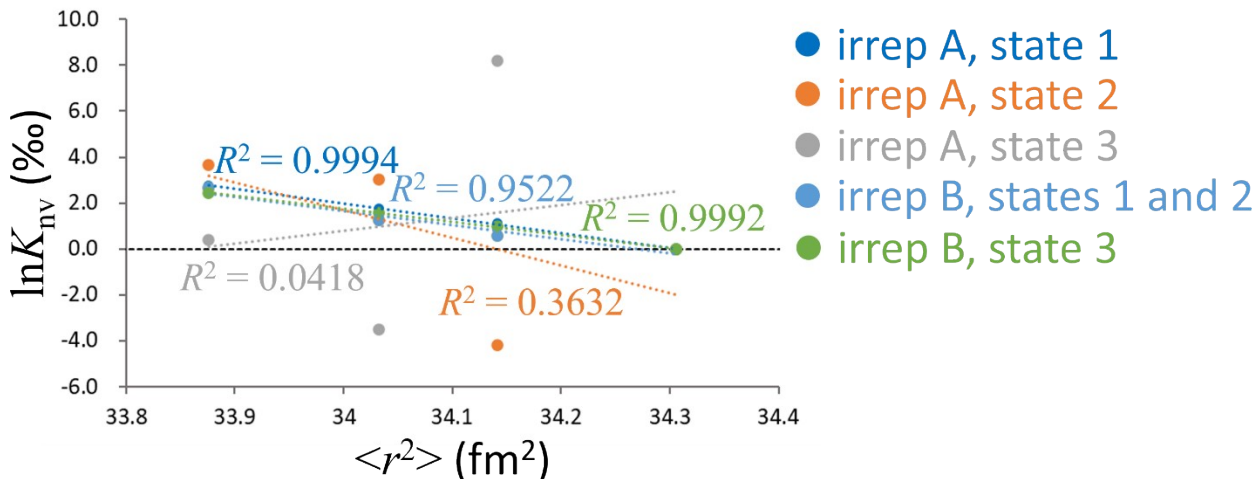


Figure S4. Relationship between $\langle r^2 \rangle$ and $\ln K_{nv}$ for the isotopes ^{233}U , ^{235}U , ^{236}U and ^{238}U for the CASPT2 method with states 1, 2 and 3 for each irrep. The horizontal axis shows $\langle r^2 \rangle$ in units of fm^2 and the vertical axis shows $\ln K_{nv}$ in units of %. The blue, orange and gray plots depict data for states 1, 2 and 3 in irrep A respectively. The light blue and yellowish green plots depict data for states 1 and 2 and 3 in irrep B. Because states 1 and 2 in irrep B were completely degenerate, they are combined into one data set. The dotted lines indicate linear regressions for each set of data, with R^2 displayed alongside these regression lines.

For the ultimate CASPT2 and RASPT2 calculations, which are free of numerical errors, MO analysis in the RAS and details of the obtained CASCI/RASCI configurations for the UCl_4 molecule are presented in Tables S7 and S8. According to Table S8, the configurations and their weights for CASCI and RASCI are almost identical, suggesting that the impact of extending the RAS is minimal. All major configurations are open-shell, i.e., two electrons occupy different Kramers pair orbitals.

Table S7 Main atomic orbital components of the RAS orbitals for the UCl_4 molecule.

RAS	Orbital energy (a.u.)	Atomic orbital	Weight (%)	Atomic orbital	Weight (%)	Atomic orbital	Weight (%)
RAS1	-0.47247	U p	21.5	Cl p	71.3	-	-
RAS1	-0.47247	U p	21.5	Cl p	65.2	-	-
RAS2 (#1)	-0.32064	U f	92.9	U d	2.4	-	-
RAS2 (#2)	-0.32064	U f	92.9	U d	1.6	-	-
RAS2 (#3)	-0.31811	U f	85.2	U s	11.1	-	-
RAS3	0.02558	U s	74.3	Cl s	23.3	-	-
RAS3	0.04930	U p	48.8	Cl s	45.9	-	-
RAS3	0.05051	U p	47.1	Cl s	47.3	U d	1.5
RAS3	0.05051	U p	47.0	Cl s	47.3	U d	2.2

Table S8 Main configurations of CASCI and RASCI wave functions. In these calculations, RAS2 and CAS shared identical orbital space. Since RAS1 and RAS3 are always doubly occupied or unoccupied in the main RASCI configurations, only the occupations of six RAS2 spinors are described. 'T' and 'F' denote occupied and unoccupied, respectively. Kramers pair orbitals, #1 to #3, correspond to those in Table S7.

Root1			CASCI energy (a.u.)		RASCI energy (a.u.)					
			-29882.4464424561		-29882.4494433251					
(#1)	(#2)	(#3)	Coeff.	Weight	Coeff.	Weight				
F	T	T	F	F	F	F	-0.697	0.485	-0.678	0.460
T	F	F	T	F	F	F	-0.697	0.485	-0.678	0.460
F	T	F	F	T	F	F	0.106	0.011	0.105	0.011
T	F	F	F	F	T	F	0.106	0.011	0.105	0.011
Root2			CASCI energy (a.u.)		RASCI energy (a.u.)					
			-29882.4456002784		-29882.4481236064					
(#1)	(#2)	(#3)	Coeff.	Weight	Coeff.	Weight				
F	T	F	F	T	F	F	-0.497	0.247	0.461	0.212
T	F	F	F	F	T	F	0.497	0.247	-0.461	0.212
F	F	F	T	T	F	F	-0.328	0.108	0.354	0.125
F	F	T	F	F	T	F	0.328	0.108	-0.354	0.125
T	T	F	F	F	F	F	-0.313	0.098	0.293	0.086
F	F	T	T	F	F	F	0.313	0.098	-0.293	0.086
F	T	T	F	F	F	F	-0.217	0.047	0.235	0.055
T	F	F	T	F	F	F	0.217	0.047	-0.235	0.055
Root3			CASCI energy (a.u.)		RASCI energy (a.u.)					
			-29882.4456002784		-29882.4481236064					
(#1)	(#2)	(#3)	Coeff.	Weight	Coeff.	Weight				
F	F	F	T	T	F	F	0.497	0.247	-0.461	0.212
F	F	T	F	F	T	F	-0.497	0.247	0.461	0.212
F	T	F	F	T	F	F	-0.328	0.108	0.354	0.125
T	F	F	F	F	T	F	0.328	0.108	-0.354	0.125
F	T	T	F	F	F	F	0.313	0.098	-0.293	0.086
T	F	F	T	F	F	F	-0.313	0.098	0.293	0.086
T	T	F	F	F	F	F	-0.217	0.047	0.235	0.055
F	F	T	T	F	F	F	0.217	0.047	-0.235	0.055

S6. Electronic energies of the ground and low-lying states

Table S9 Electronic energies of the ground and low-lying states. The “-” symbol indicates that

calculations were not performed.

	Irrep	State 1	State 2	State 3
CCSD	A	-29883.44141883	-	-
	B	-29883.46259390	-	-
CCSD(T)	A	-29883.49173105	-	-
	B	-29883.50414108	-	-
FSCCSD	A	-29883.35479853	-29883.34967038	-29883.34723354
	B	-29883.34967038	-29883.34967038	-29883.33908861
CASCI	A	-29882.44644246	-29882.44560028	-29882.44560028
	B	-29882.44644246	-29882.44644246	-29882.44456160
CASPT2	A	-29883.42983856	-29883.42892713	-29883.42907339
	B	-29883.42983802	-29883.42983802	-29883.42823502
RASCI	A	-29882.44944333	-29882.44812361	-29882.44812361
	B	-	-	-
RASPT2	A	-29883.42868862	-	-
	B	-	-	-

S7. Configuration analysis of FSCCD results

Initially, the occupancies of f orbitals in virtual MOs designated as the Fock space were assessed by analyzing the proportion of f orbitals in these MOs. Table S10 presents these proportions alongside the corresponding orbital energies. Subsequently, the contribution of each configuration to the ground state was investigated, as summarized in Table 11.

Table S10 Orbital energy values and proportional occupations of f orbitals for each MO specified as the Fock space as used in the FSCCD calculations. The orbital energies have units of E_h .

UF ₄	Orbital energy	Proportion of f orbitals
MO1	-0.6370962247193	84.56 %
MO2	-0.6370962246377	79.93 %
MO3	-0.6359521148321	42.97 %
MO4	-0.6049736344027	83.27 %
MO5	-0.6004036886342	83.76 %
MO6	-0.6004036884238	82.69 %
MO7	-0.5972712316163	43.13 %

UCl ₄	Orbital energy	Proportion of f orbitals
MO1	-0.5275427331659	59.99 %
MO2	-0.5064576685500	71.69 %
MO3	-0.5064576683664	71.70 %
MO4	-0.4619818990009	71.59 %
MO5	-0.4606907119611	79.14 %
MO6	-0.4606907118840	79.15 %
MO7	-0.4567845757738	83.64 %

Table S11 Coefficients of contributing configurations to the ground state as used in the FSCCD calculations. The number of each MO corresponds to that in Table S8.

UF ₄ Coefficient	Fock space MOs in which two electrons are added (irrep in C ₂)
-0.684	MO1 (¹ E), MO2 (² E)
0.684	MO2 (¹ E), MO1 (² E)
0.133	MO2 (¹ E), MO4 (² E)
-0.133	MO4 (¹ E), MO2 (² E)

UCl ₄ Coefficient	Fock space MOs in which two electrons are added (irrep in C ₂)
-0.857	MO1 (¹ E), MO1 (² E)
0.363	MO2 (¹ E), MO2 (² E)
0.363	MO3 (¹ E), MO3 (² E)

S8. T_1 , T_2 amplitudes obtained from CCSD calculations for UCl_4

Table S12 Single and double electron excitation amplitudes (T_1 and T_2) for UCl_4 obtained from the CCSD calculations. The values in parentheses indicate the proportion of components in the MO, with only those exceeding 10 % shown here.

T_1 amplitude	Main components of MO from which electron is excited	Main components of MO to which electron is excited
0.2186	<i>Uf</i> (92.9 %)	<i>Uf</i> (85.2 %), <i>Us</i> (11.1 %)
-0.1241	<i>Uf</i> (92.9 %)	<i>Uf</i> (85.2 %), <i>Us</i> (11.1 %)
-0.0694	<i>Uf</i> (92.9 %)	<i>Cl s</i> (67.9 %), <i>U d</i> (11.1 %)
-0.0514	<i>Uf</i> (92.9 %)	<i>Cl s</i> (54.8 %)
0.0505	<i>Cl p</i> (98.0 %)	<i>Uf</i> (85.2 %), <i>Us</i> (11.1 %)
0.0485	<i>Cl p</i> (98.0 %)	<i>Uf</i> (85.2 %), <i>Us</i> (11.1 %)
0.0424	<i>Cl p</i> (96.9 %)	<i>Cl s</i> (38.6 %), <i>U d</i> (20.8 %), <i>U p</i> (15.6 %), <i>Cl p</i> (11.6 %)
0.0421	<i>Cl p</i> (92.8 %)	<i>Cl s</i> (38.6 %), <i>U d</i> (20.9 %), <i>U p</i> (15.6 %), <i>Cl p</i> (11.6 %)
-0.0394	<i>Uf</i> (92.9 %)	<i>Cl s</i> (67.9 %), <i>U d</i> (11.1 %)
-0.0359	<i>Uf</i> (92.9 %)	<i>Cl s</i> (54.6 %), <i>Cl p</i> (11.6 %)
0.0338	<i>Cl p</i> (92.8 %)	<i>Cl s</i> (38.6 %), <i>U d</i> (20.9 %), <i>U p</i> (15.6 %), <i>Cl p</i> (11.6 %)
0.0335	<i>Cl p</i> (96.9 %)	<i>Cl s</i> (38.6 %), <i>U d</i> (20.8 %), <i>U p</i> (15.6 %), <i>Cl p</i> (11.6 %)
-0.0329	<i>Uf</i> (92.9 %)	<i>Cl s</i> (53.8 %), <i>U p</i> (18.8 %), <i>U d</i> (14.4 %)
-0.0328	<i>Uf</i> (92.9 %)	<i>Cl s</i> (67.1 %), <i>U p</i> (21.3 %)

Continued

T_2 amplitude	Main components of two MOs from which electrons are excited		Main components of two MOs to which electrons are excited	
0.0199	<i>Uf</i> (92.9 %)	<i>Uf</i> (92.9 %)	<i>Cl s</i> (67.9 %), <i>U d</i> (11.1 %)	<i>Uf</i> (92.9 %)
0.0188	<i>Uf</i> (92.9 %)	<i>Uf</i> (92.9 %)	<i>Cl s</i> (54.6 %), <i>Cl p</i> (11.6 %)	<i>Uf</i> (85.2 %), <i>U s</i> (11.1 %)
-0.0158	<i>Uf</i> (92.9 %)	<i>Uf</i> (92.9 %)	<i>Cl s</i> (54.8 %), <i>Cl p</i> (16.3 %)	<i>Uf</i> (92.9 %)
-0.0151	<i>Up</i> (99.0 %)	<i>Up</i> (99.0 %)	<i>Uf</i> (85.2 %), <i>U s</i> (11.1 %)	<i>Uf</i> (85.2 %), <i>U s</i> (11.1 %)
-0.0142	<i>Cl p</i> (92.8 %)	<i>Cl p</i> (92.8 %)	<i>Cl s</i> (38.6 %), <i>U d</i> (20.9 %), <i>U p</i> (15.6 %), <i>Cl p</i> (11.6 %)	<i>Cl s</i> (38.6 %), <i>U d</i> (20.9 %), <i>U p</i> (15.6 %), <i>Cl p</i> (11.6 %)
-0.0142	<i>Cl p</i> (96.9 %)	<i>Cl p</i> (96.9 %)	<i>Cl s</i> (38.6 %), <i>U d</i> (20.8 %), <i>U p</i> (15.6 %), <i>Cl p</i> (11.6 %)	<i>Cl s</i> (38.6 %), <i>U d</i> (20.8 %), <i>U p</i> (15.6 %), <i>Cl p</i> (11.6 %)
-0.0137	<i>Uf</i> (92.9 %)	<i>Uf</i> (92.9 %)	<i>Cl s</i> (54.8 %), <i>Cl p</i> (16.3 %)	<i>Cl s</i> (67.9 %), <i>U d</i> (11.1 %)
0.0113	<i>Uf</i> (92.9 %)	<i>Uf</i> (92.9 %)	<i>Cl s</i> (67.9 %), <i>U d</i> (11.1 %)	<i>Uf</i> (92.9 %)
-0.0106	<i>Uf</i> (92.9 %)	<i>Uf</i> (92.9 %)	<i>Cl s</i> (54.6 %), <i>Cl p</i> (11.6 %)	<i>Uf</i> (92.9 %)
0.0101	<i>Uf</i> (92.9 %)	<i>Uf</i> (92.9 %)	<i>Cl s</i> (67.1 %), <i>U p</i> (21.3 %)	<i>Uf</i> (92.9 %)

Supplementary Information References

1. G. Scalmani and M. J. Frisch, Continuous surface charge polarizable continuum models of solvation. I. General formalism, *J. Chem. Phys.*, 2010, **132**(11), 144110, DOI: 10.1063/1.3359469.
2. M. J. Frisch, G. W. Trucks, H. B. Schlegel, G. E. Scuseria, M. A. Robb, J. R. Cheeseman, G. Scalmani, V. Barone, G. A. Petersson, H. Nakatsuji, X. Li, M. Caricato, A. Marenich, J. Bloino, B. G. Janesko, R. Gomperts, B. Mennucci, H. P. Hratchian, J. V. Ortiz, A. F. Izmaylov, J. L. Sonnenberg, D. Williams-Young, F. Ding, F. Lipparini, F. Egidi, J. Goings, B. Peng, A. Petrone, T. Henderson, D. Ranasinghe, V. G. Zakrzewski, J. Gao, N. Rega, G. Zheng, W. Liang, M. Hada, M. Ehara, K. Toyota, R. Fukuda, J. Hasegawa, M. Ishida, T. Nakajima, Y. Honda, O. Kitao, H. Nakai, T. Vreven, K. Throssell, J. A. Montgomery, Jr., J. E. Peralta, F. Ogliaro, M. Bearpark, J. J. Heyd, E. Brothers, K. N. Kudin, V. N. Staroverov, T. Keith, R. Kobayashi, J. Normand, K. Raghavachari, A. Rendell, J. C. Burant, S. S. Iyengar, J. Tomasi, M. Cossi, J. M. Millam, M. Klene, C. Adamo, R. Cammi, J. W. Ochterski, R. L. Martin, K. Morokuma, O. Farkas, J. B. Foresman, and D. J. Fox, Gaussian09, Revision A.02: Gaussian, Inc., Wallingford CT, USA, 2009.
3. A. Sato, R. Bernier-Latmani, M. Hada, and M. Abe, Ab initio and steady-state models for uranium isotope fractionation in multi-step biotic and abiotic reduction, *Geochim. Cosmochim. Acta*, 2021, **307**, 212–227, DOI: 10.1016/j.gca.2021.05.044.
4. C. Møller and M. S. Plesset, Note on an approximation treatment for many-electron systems, *Phys. Rev.*, 1934, **46**(7), 618–622, DOI: 10.1103/PhysRev.46.618.
5. J. N. P. van Stralen, L. Visscher, C. V. Larsen, and H. J. A. Jensen, First-order MP2 molecular properties in a relativistic framework, *Chem. Phys.*, 2005, **311**, 81–95, DOI: 10.1016/j.chemphys.2004.10.018.
6. L. Visscher, T. J. Lee, and K. G. Dyall, Formulation and implementation of a relativistic unrestricted coupled-cluster method including noniterative connected triples, *J. Chem. Phys.*, 1996, **105**(19), 8769–8776, DOI: 10.1063/1.472655.
7. A. Shee, L. Visscher, and T. Saue, Analytic one-electron properties at the 4-component relativistic coupled cluster level with inclusion of spin-orbit coupling, *J. Chem. Phys.*, **145**(18), 184107, DOI: 10.1063/1.4966643.
8. L. Visscher, E. Eliav, and U. Kaldor, Formulation and implementation of the relativistic Fock-space coupled cluster method for molecules, *J. Chem. Phys.*, 2001, **115**(21), 9720–9726, DOI: 10.1063/1.1415746.
9. M. Iliaš and T. Saue, An infinite-order two-component relativistic Hamiltonian by a simple one-step transformation, *J. Chem. Phys.*, 2007, **126**(6), 064102, DOI: 10.1063/1.2436882.
10. W. Liu, Ideas of relativistic quantum chemistry, *Mol. Phys.*, 2010, **108**(13), 1679–1706, DOI: 10.1080/00268971003781571.

11. T. Saue, Relativistic Hamiltonians for chemistry: A primer, *ChemPhysChem.*, 2011, **12**(17), 3077–3094, DOI: 10.1002/cphc.201100682.
12. S. Knecht, M. Repisky, H. J. A. Jensen, and T. Saue, Exact two-component Hamiltonians for relativistic quantum chemistry: Two-electron picture-change corrections made simple, *J. Chem. Phys.*, 2022, **157**(11), 114106, DOI: 10.1063/5.0095112.
13. K. G. Dyall, Relativistic double-zeta, triple-zeta, and quadruple-zeta basis sets for the actinides Ac–Lr, *Theor. Chem. Acc.*, 2007, **117**, 491–500, DOI: 10.1007/s00214-006-0175-4.
14. R. Ditchfield, W. J. Hehre, and J. A. Pople, Self-consistent molecular-orbital methods. IX. An extended gaussian-type basis for molecular-orbital studies of organic molecules, *J. Chem. Phys.*, 1971, **54**(2), 724–728, DOI: 10.1063/1.1674902.
15. T. H. Dunning Jr., Gaussian basis functions for use in molecular calculations. IV. The representation of polarization functions for the first row atoms and hydrogen, *J. Chem. Phys.*, 1971, **55**(8), 3958–3966, DOI: 10.1063/1.1676685.
16. W. J. Hehre, R. Ditchfield, and J. A. Pople, Self-consistent molecular orbital methods. XII. Further extensions of gaussian-type basis sets for use in molecular orbital studies of organic molecules, *J. Chem. Phys.*, 1972, **56**(5), 2257–2261, DOI: 10.1063/1.1677527.
17. P. C. Hariharan and J. A. Pople, The influence of polarization functions on molecular orbital hydrogenation energies, *Theor. Chim. Acta*, 1973, **28**, 213–222, DOI: 10.1007/BF00533485.
18. K. G. Dyall, Relativistic double-zeta, triple-zeta, and quadruple-zeta basis sets for the light elements H–Ar, *Theor. Chem. Acc.*, 2016, **135**, 128, DOI: 10.1007/s00214-016-1884-y.
19. C. Lee, W. Yang, and R. G. Parr, Development of the Colle-Salvetti correlation-energy formula into a functional of the electron density, *Phys. Rev. B*, 1988, **37**(2), 785–789, DOI: 10.1103/PhysRevB.37.785.
20. A. D. Becke, Density-functional thermochemistry. III. The role of exact exchange, *J. Chem. Phys.*, 1993, **98**(7), 5648–5652, DOI: 10.1063/1.464913.
21. P. J. Stephens, F. J. Devlin, C. F. Chabalowski, and M. J. Frisch, Ab initio calculation of vibrational absorption and circular dichroism spectra using density functional force fields, *J. Phys. Chem.*, 1994, **98**(45), 11623–11627, DOI: 10.1021/j100096a001.
22. K. Andersson, P. -Å. Malmqvist, B. O. Roos, A. J. Sadlej, and K. Wolinski, Second-order perturbation theory with a CASSCF reference function, *J. Phys. Chem.*, 1990, **94**(14), 5483–5488, DOI: 10.1021/j100377a012.
23. K. Andersson, P. -Å. Malmqvist, and B. O. Roos, Second-order perturbation theory with a complete active space self-consistent field reference function, *J. Chem. Phys.*, 1992, **96**(2), 1218–1226, DOI: 10.1063/1.462209.
24. M. Abe, T. Nakajima, and K. Hirao, The relativistic complete active-space second-order perturbation theory with the four-component Dirac Hamiltonian, *J. Chem. Phys.*, 2006, **125**(23), 234110, DOI: 10.1063/1.2404666.
25. P. Å. Malmqvist, K. Pierloot, A. R. M. Shahi, C. J. Cramer, and L. Gagliardi, The restricted

active space followed by second-order perturbation theory method: Theory and application to the study of CuO_2 and Cu_2O_2 systems, *J. Chem. Phys.*, 2008, **128**(20), 204109, DOI: 10.1063/1.2920188.

26. T. Saue, R. Bast, A. S. P. Gomes, H. J. A. Jensen, L. Visscher, I. A. Aucar, R. Di Remigio, K. G. Dyall, E. Eliav, E. Fasshauer, T. Fleig, L. Halbert, E. D. Hedegård, B. Helmich-Paris, M. Iliaš, C. R. Jacob, S. Knecht, J. K. Laerdahl, M. L. Vidal, M. K. Nayak, M. Olejniczak, J. M. H. Olsen, M. Pernpointner, B. Senjean, A. Shee, A. Sunaga, and J. N. P. van Stralen, The DIRAC code for relativistic molecular calculations, *J. Chem. Phys.*, **152**(20), 204104, DOI: 10.1063/5.0004844.
27. R. Bast, A.S.P. Gomes, T. Saue, L. Visscher, H.J.A. Jensen, I.A. Aucar, V. Bakken, K.G. Dyall, S. Dubillard, U. Ekström, E. Eliav, T. Enevoldsen, E. Faßhauer, T. Fleig, O. Fossgaard, L. Halbert, E.D. Hedegård, T. Helgaker, B. Helmich-Paris, J. Henriksson, M. Iliaš, C.R. Jacob, S. Knecht, S. Komorovský, O. Kullie, J.K. Lærdahl, C.V. Larsen, Y.S. Lee, N.H. List, H.S. Nataraj, M.K. Nayak, P. Norman, G. Olejniczak, J. Olsen, J.M.H. Olsen, A. Papadopoulos, Y.C. Park, J.K. Pedersen, M. Pernpointner, J.V. Pototschnig, R. Di Remigio, M. Repiský, K. Ruud, P. Sałek, B. Schimmelpfennig, B. Senjean, A. Shee, J. Sikkema, A. Sunaga, A.J. Thorvaldsen, J. Thyssen, J. van Stralen, M.L. Vidal, S. Villaume, O. Visser, T. Winther, and S. Yamamoto, DIRAC21 (Zenodo, 2021).